Available online at www.sciencedirect.com
SCIENCE DIRECT
Aerospace Science and Technology 10 (2006) 385–393
Aerospace Science and Technology
www.elsevier.com/locate/aescte

Numerical investigation of the shock interaction effect on the lateral jet controlled missile

Byung-Young Min [1], Jae-Woo Lee [*,2], Yung-Hwan Byun [3]

Center for Advanced e-System Integration Technology, Konkuk University, 1 Hwayang, Gwangjin, Seoul 143-701, South Korea

Received 22 July 2005; received in revised form 11 November 2005; accepted 16 November 2005

Available online 6 February 2006

Abstract

A computational study on the supersonic flow around the lateral jet controlled missile has been performed. A three-dimensional Navier–Stokes computer code (AADL 3D) has been developed and case studies have been performed by comparing the normal force coefficient and the moment coefficient of a missile body. Different jet flow conditions including jet pressures and jet Mach numbers, and the circumferential jet positions have been incorporated into the case studies. The missile surface is divided into four regions with respect to the center of gravity, and the normal force and moment distribution at each region are compared. The results show conspicuously different normal force and moment variations according to each parameter variation. From the detailed flow field analyses, it has been verified that most of the normal force loss and the pitching moment generation are taking place at the low-pressure region behind the jet nozzle. Furthermore, it is shown that the pitching moment can be efficiently reduced by the lateral thrust obtained through higher jet Mach number rather than high jet pressure. Thus, an angle of yaw is more effective for missile control by side jet than an angle of attack.

Keywords: Lateral jet; Jet nozzle; Navier–Stokes equations; Missile control

1. Introduction

Missiles have achieved rapid growth through the cold war since the first military missiles, V-1 and V-2, developed by Germany during the World War II. Therefore, it has become necessary to develop a defense system to counteract missiles, especially guided missiles such as ballistic missiles. Since the seventies, attacking missiles have been outfitted with a ramjet engine due to its excellent performance at low altitude and high velocity [4]. This requires any missile defense system to have even greater maneuverability. Existing fin controlled missiles have delayed response time and limitations on maneuvering at low velocity or high altitude. These missiles are controlled by the moments produced at the control surfaces that need high dynamic pressure. However, the lateral jet controlled missiles have short response time and high maneuverability even at low velocity and low-density area. Therefore, the lateral jet attitude control has been a preferred concept for a new missile defense system. However, it also has drawbacks like operating time restriction because of the space limitation for jet propellant and abstruseness of analysis due to complicated flow structure caused by freestream–jet interaction [7].

Two types of missile attitude control using lateral jet can be considered (Fig. 1). First, by locating the jet at the center of gravity of the missile, a parallel transition movement of missile (Fig. 1(a)) can be obtained by avoiding pitching moment generation. The other type is to control the missile attitude using the pitching moment generated by the jet located at a certain distance from the missile center of gravity (Fig. 1(b)).

As shown in Fig. 2, the dominant aerodynamic characteristic of a flow around the lateral jet is described by the local shock–shock interaction, which consists of separation shock, bow shock, barrel shock and Mach disk around jet nozzle, and the downstream interaction by the counter rotating vortices [1,7]. By the bow shock, shock–boundary layer interaction, and separation shock, a high-pressure region is formed in front of

* Corresponding author. Tel.: +82 2 450 3461, fax: +82 2 444 6670.
E-mail address: jwlee@konkuk.ac.kr (J.-W. Lee).
[1] Graduate Research Assistant, Department of Aerospace Engineering.
[2] Associate Professor, Department of Aerospace Engineering.
[3] Professor, Department of Aerospace Engineering.

1270-9638/$ – see front matter
doi:10.1016/j.ast.2005.11.013

Nomenclature

C_M	moment coefficient ($C_M = M/qSd$)	S	missile cross-sectional area ..... m^2
C_N	normal force coefficient ($C_N = N/qS$)	T_{jet}	jet thrust ..... N
C_P	pressure coefficient	α	angle of attack ..... deg
C_T	thrust coefficient ($C_T = T_{jet}/qS$)	θ	circumferential angle around the missile body deg
C.G.	center of gravity		
d	missile diameter ..... m	*Subscripts*	
M_{jet}	jet Mach number	FU	forebody upper-side of missile
$\dot{m}_{jet}$	mass flow rate of jet ..... kg/s	FL	forebody lower-side of missile
N	normal force ..... N	jet	jet-on condition
P_∞	freestream pressure	jetoff	jet-off condition
P_{jet}	jet pressure	RU	rear body upper-side of missile
P_{ratio}	jet pressure ratio ($P_{ratio} = P_{jet}/P_\infty$)	RL	rear body lower-side of missile
q	dynamic pressure	∞	freestream condition

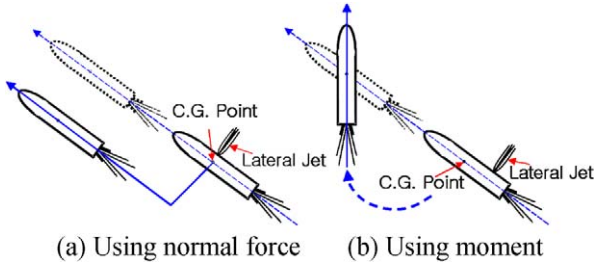

Fig. 1. Missile attitude control using lateral jet.

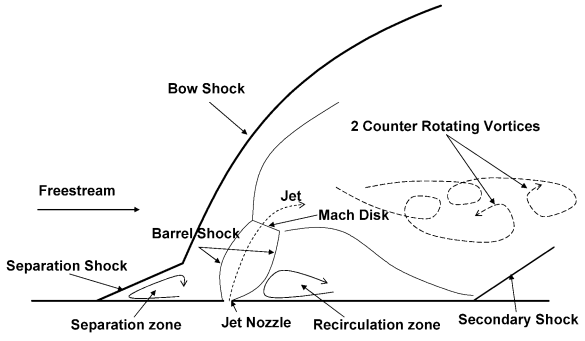

Fig. 2. Complicated flow structure around jet nozzle.

the lateral jet nozzle. A low-pressure region is generated behind the jet nozzle due to the suction effect caused by the lateral jet and the two counter rotating vortices. Therefore, a pitch down moment is generated around the jet nozzle, which is located at the center of gravity of the missile. The propagated vortices produce unexpected effects due to the interaction between the vortices and projected parts such as the fin or the wing. In case of high jet pressure ratio, when the lateral jet is applied to the three-dimensional bodies such as missiles, the bow shock in front of the jet nozzle wraps around the body. This generates a high-pressure region at the opposite side of jet nozzle, which reduces the lateral jet performance [2,11]. These phenomena are affected by the jet, and the size of the barrel shock increases as the jet pressure and the jet Mach number increase [1]. Therefore, the jet flow condition has a direct impact on the flow structure formed by the shock interaction.

Brandeis and Gill [2] examined the effect of jet injection angles and several nozzle shapes by wind tunnel test. The nozzle shapes included were circular, rectangular and multiple nozzles. It was found that the jet injection nozzle shape and vector angle can have a noticeable effect on the magnitude of the jet force amplification. Chamberlain [3] solved three-dimensional hypersonic jet interaction problem for a generic interceptor configuration at zero degrees angle of attack using Navier–Stokes equations with Roe's scheme and analyzed detailed complex flow structure. Roger and Chan [9,10] performed systematic CFD analyses for configuration of flat plate with a single jet, of square crossection, exiting into a supersonic cross flow to investigate the influence of jet Mach number and approach boundary layer thickness on the vertical penetration distance of the jet. Roger and Chan found that, if the jet penetration is higher than the boundary layer thickness, the penetration of jet plumes increases with jet Mach number from 1 to 3, assuming fixed jet total conditions and mass flow rate. Roger and Chan also observed the jet Mach number effect on the plume size, plume penetration angle, and the bow shock separation from the barrel shock. Srivastava [11] has shown the effect of jet thrust, jet position, and jet angle on the amplification factor of the missile through several case studies. However, the effects of jet pressure and jet Mach number were not considered separately, and the case studies consist of windward and leeward cases only. Besides, there is no systematic study on the pitch moment variation around the jet nozzle, which is most critical factor in the type Fig. 1(a), with respect to the jet flow condition and the jet position.

In this study, type Fig. 1(a), a lateral jet located at the center of gravity, is considered. Therefore, the pitching moment generation is a negative effect to the missile control and should be diminished.

In this paper, a systematic approach for investigating the effects of jet flow conditions including jet pressure, jet Mach number, and jet mass flow rate on the aerodynamic characteristics of the missile is outlined. This is accomplished by comparing the normal force coefficient and the moment coefficient at the corresponding jet flow conditions. Concurrently, the cir-

cumferential jet position effect is investigated when the missile has an angle of attack, to investigate the different freestream angle effect. Furthermore, the missile is divided into four regions, and the normal force and moment contributions are compared to determine the most important part being considered for an efficient missile design. Although the nozzle shape is also important parameter, since this study is focused on the jet flow condition and the position effects, circular nozzle shape is used for all cases as a basis. A three-dimensional Navier–Stokes computer code (AADL 3D) has been developed and validated to simulate the complex flow around a lateral jet controlled missile.

2. Aerodynamic analysis method

2.1. Governing equations

A three-dimensional Navier–Stokes computer code, AADL 3D, is developed for the analysis of complex flow phenomena around the lateral jet controlled missile. These equations for the computational domain are shown in Eqs. (1)–(3). The spatial flux vectors **E**, **F**, **G**, and viscous terms $\mathbf{E}_v$, $\mathbf{F}_v$ and $\mathbf{G}_v$ are given by Eq. (2), using contravariant velocities U, V, and W.

$$\frac{\partial \mathbf{Q}}{\partial t} + \frac{\partial \mathbf{E}}{\partial \xi} + \frac{\partial \mathbf{F}}{\partial \eta} + \frac{\partial \mathbf{G}}{\partial \zeta} = \frac{\partial \mathbf{E}_v}{\partial \xi} + \frac{\partial \mathbf{F}_v}{\partial \eta} + \frac{\partial \mathbf{G}_v}{\partial \zeta}, \tag{1}$$

$$\mathbf{Q} = \frac{1}{J}\begin{Bmatrix} \rho \\ \rho u \\ \rho v \\ \rho w \\ e_t \end{Bmatrix}, \qquad \mathbf{E} = \frac{1}{J}\begin{Bmatrix} \rho U \\ \rho u U + \xi_x p \\ \rho v U + \xi_y p \\ \rho w U + \xi_z p \\ (e_t + p)U \end{Bmatrix},$$

$$\mathbf{F} = \frac{1}{J}\begin{Bmatrix} \rho V \\ \rho u V + \eta_x p \\ \rho v V + \eta_y p \\ \rho w V + \eta_z p \\ (e_t + p)V \end{Bmatrix}, \qquad \mathbf{G} = \frac{1}{J}\begin{Bmatrix} \rho W \\ \rho u W + \zeta_x p \\ \rho v W + \zeta_y p \\ \rho w W + \zeta_z p \\ (e_t + p)W \end{Bmatrix},$$

$$\mathbf{E}_v = \frac{1}{J R_a}\begin{Bmatrix} 0 \\ \xi_x \tau_{xx} + \xi_y \tau_{yx} + \xi_z \tau_{zx} \\ \xi_x \tau_{xy} + \xi_y \tau_{yy} + \xi_z \tau_{zy} \\ \xi_x \tau_{xz} + \xi_y \tau_{yz} + \xi_z \tau_{zz} \\ \xi_x \beta_x + \xi_y \beta_y + \xi_z \beta_z \end{Bmatrix},$$

$$\mathbf{F}_v = \frac{1}{J R_a}\begin{Bmatrix} 0 \\ \eta_x \tau_{xx} + \eta_y \tau_{yx} + \eta_z \tau_{zx} \\ \eta_x \tau_{xy} + \eta_y \tau_{yy} + \eta_z \tau_{zy} \\ \eta_x \tau_{xz} + \eta_y \tau_{yz} + \eta_z \tau_{zz} \\ \eta_x \beta_x + \eta_y \beta_y + \eta_z \beta_z \end{Bmatrix}, \tag{2}$$

$$\mathbf{G}_v = \frac{1}{J R_a}\begin{Bmatrix} 0 \\ \zeta_x \tau_{xx} + \zeta_y \tau_{yx} + \zeta_z \tau_{zx} \\ \zeta_x \tau_{xy} + \zeta_y \tau_{yy} + \zeta_z \tau_{zy} \\ \zeta_x \tau_{xz} + \zeta_y \tau_{yz} + \zeta_z \tau_{zz} \\ \zeta_x \beta_x + \zeta_y \beta_y + \zeta_z \beta_z \end{Bmatrix},$$

$$\begin{aligned} \beta_x &= u\tau_{xx} + v\tau_{xy} + w\tau_{xz} - q_x, \\ \beta_y &= u\tau_{yx} + v\tau y_{yy} + w\tau y_{yz} - q_y, \\ \beta_z &= u\tau_{zx} + v\tau y_{zy} + w\tau y_{zz} - q_z. \end{aligned} \tag{3}$$

In these equations, **Q** is the conservative variable vector; ρ is the density of the air; p is the pressure; u, v and w are the velocity components; e_t is the total energy per unit mass; J is the Jacobian from the coordinate transformation; R_a is the Reynolds number based on the sonic velocity; τ is the shear stress; and q_x, q_y, q_z represent the heat flux.

The Spalart–Allmaras one-equation turbulence model is implemented in the AADL 3D code, for relatively rapid computational time [6].

Roe's Flux Difference Splitting (FDS) scheme is implemented for the spatial discretization with the Monotonic Upstream-Centered Scheme for Conservation Laws (MUSCL) [5] for higher order extension. The minmod limiter [5] is used to remove solution oscillations. Central difference scheme is used for the calculation of viscous flux term, while the fully implicit Lower-Upper Symmetric-Gauss–Seidal Algorithm (LU-SGS) scheme [12] is employed for time integration.

2.2. Validation of the numerical approach

2.2.1. Ogive-cylinder body

To check whether the developed code correctly predicts the supersonic flow field around the missile body, the calculated surface pressure distributions on an ogive-cylinder body are compared with the experimental measurement results of Edward W. Perkins and Leland H. Jorgensen [8] at angles of attack of 0°, 5°, 10°. The freestream Mach number and the Reynolds number are 1.98 and 0.39×10^6, respectively. The computational grid is $70 \times 40 \times 40$ for a half-body. The geometry of an ogive-cylinder body and corresponding grid system are shown in Fig. 3.

The comparison of pressure coefficients between computational results and experimental data are shown in Figs. 4 and 5. The experimental investigation was conducted in the Ames 1-by 3-foot supersonic wind tunnel [8]. The value along the axial distance is shown in Fig. 4, where $\alpha = 0°$ and $\alpha = 180°$ represent windward and leeward side, respectively. The axial

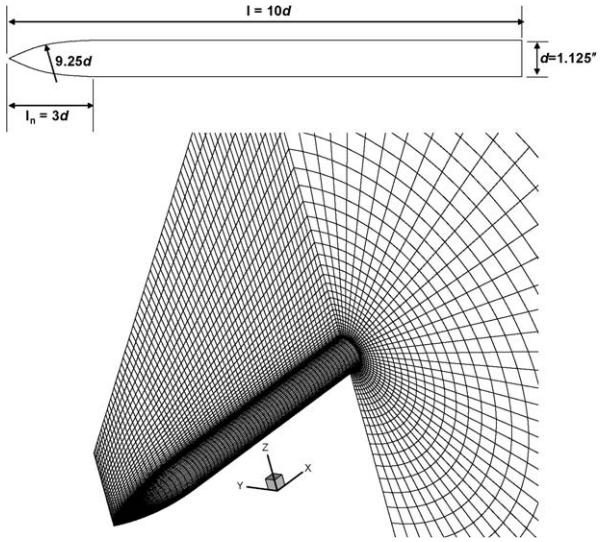

Fig. 3. The geometry and grid system of ogive-cylinder body for the code validation.

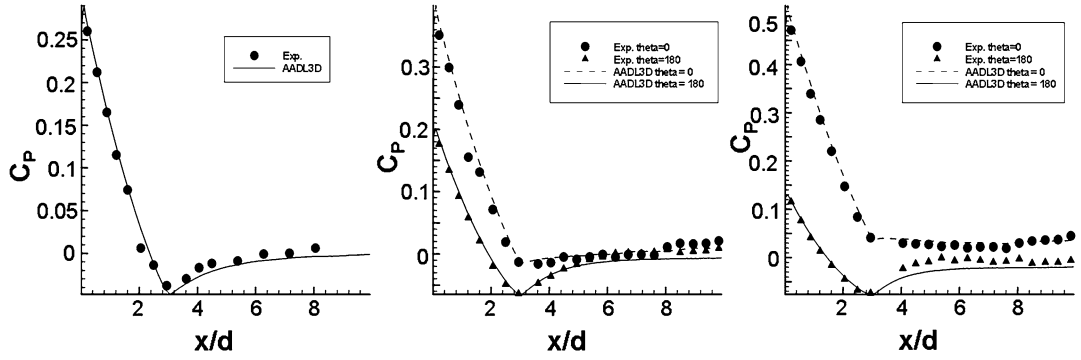

(a) $\alpha = 0^\circ$ (b) $\alpha = 5^\circ$ (c) $\alpha = 10^\circ$

Fig. 4. Comparison of surface pressure coefficients along the axial direction ($M_\infty = 1.98$, $Re = 0.39 \times 10^6$).

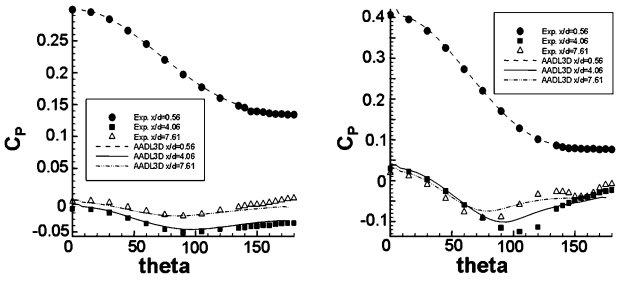

(a) $\alpha = 5^\circ$ (b) $\alpha = 10^\circ$

Fig. 5. Comparison of surface pressure coefficients along the circumferential direction.

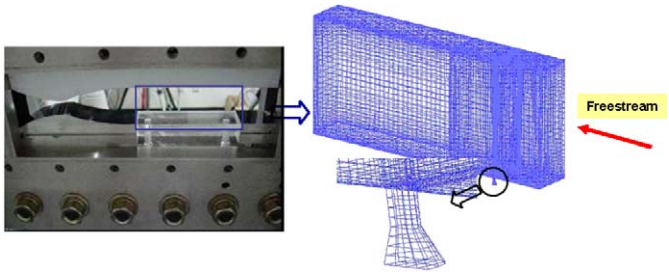

Fig. 6. The experimental setup and computational grid systems.

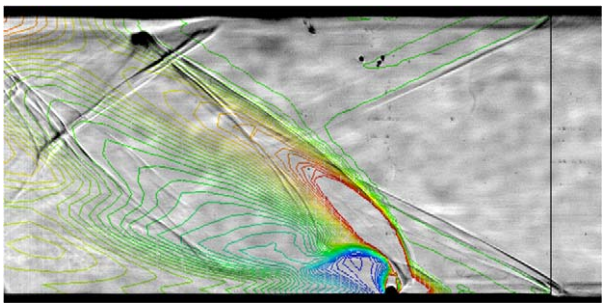

Fig. 7. Shock structure comparison (pressure contour).

distance is nondimensionalized by the diameter of cylinder. The value along the circumferential angles between 0°–180° is shown in Fig. 5. At the angle of attack of 10°, the numerically predicted separation point is a little different from the experimental data at the leeward side but at the windward side and near the nose, the agreement is excellent. Overall computational results are in good agreement with the experimental data.

2.2.2. *Sonic jet on the flat plate*

Sonic jet ejection on the flat plate in the supersonic flow field has been analyzed to verify the freestream-jet interaction analysis capability of AADL 3D through an experiment conducted in the Konkuk University micro-supersonic wind tunnel. The experimental conditions are given by $P_{ratio} = 80$; $M_\infty = 2.5$; $M_{jet} = 1.0$; jet total pressure, 4.5 MPa; Reynolds number, 5.66×10^5. The micro-supersonic wind tunnel at Konkuk University is designed for educational purpose only, and therefore, force and moment could not be obtained. Thus, only the shock structure is compared with the experimental flow visualization result. The experimental setup and generated grid system are shown in Fig. 6, where the grid system consists of 85,150 cells.

The symmetry plane analysis results are shown overlapping on the flow visualization results in Fig. 7. While the analysis results consider only the symmetry plane, the flow visualization results consider all the shock structures in three-dimensional space. The barrel shock, separation zone and bow shock structures are in good agreement with experimental results.

3. Case studies of lateral jet controlled missile

3.1. *Grid system selection*

The missile configuration for the case studies is a simple tangent ogive-cylinder body without a fin, as shown in Fig. 8. A grid system, which is coarse but guarantees solution accuracy, is selected by investigating the convergence rate and the converged solutions of several grid systems. This grid system also leads to greater computational efficiency. The chamber condition of the lateral jet and the inside contour of the jet nozzle effects are ignored to facilitate analyses. Thus, the lateral jet flow condition is set on the nozzle exit plane as a fixed boundary condition.

M_∞ is 2.6 and M_{jet} is 2.04. P_{ratio} is 45.7 and the Reynolds number is 6.63×10^6. The 10 km standard atmospheric condition is used as the ambient condition. For an optimum combination of computational time and accuracy, the $95 \times 34 \times 33$ grid system containing 106,590 cells is selected, since it has only

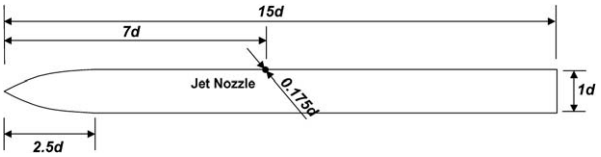

Fig. 8. Missile configuration for the case studies.

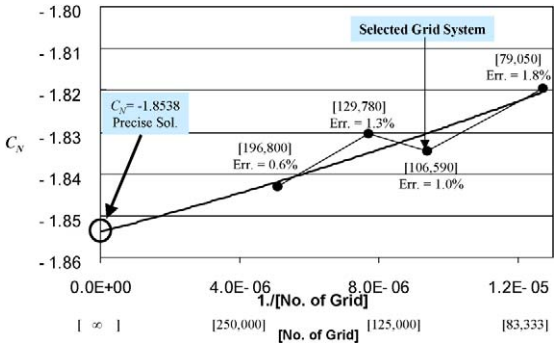

Fig. 9. The result of grid density test.

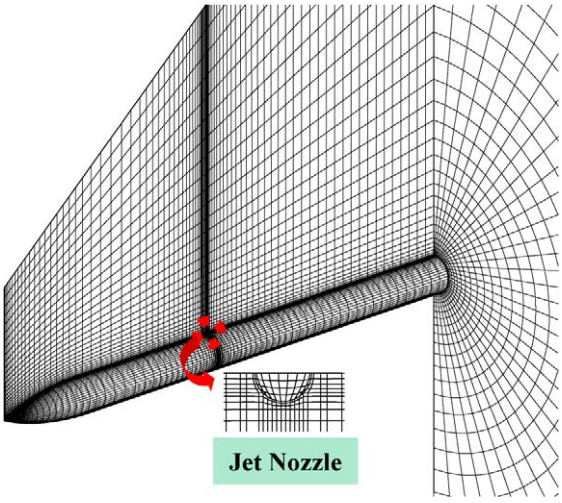

Fig. 10. Selected grid system (95 × 34 × 33).

1% error as shown in Fig. 9. A quadratic polynomial equation is used to regress obtained data and then extrapolated to estimate exact value. The grid system is shown in Fig. 10.

3.2. Freestream and analysis conditions

The normal force and the moment coefficients of a missile body are compared to determine the effect of the jet flow characteristics on the missile attitude for different pressure ratios and jet Mach number variations. For all calculations at different jet flow condition effects, the analysis condition of freestream flow is the same as the grid system selection case, where Table 1 summarizes the jet flow conditions for each case.

The missile configuration is nondimensionalized by the missile diameter, d. Parameters like force and moment are shown in Fig. 11. The missile surface is divided into four regions with respect to the center of gravity, and the normal force and moment distribution in each region are compared.

Table 1
Jet flow conditions

	Case 1	Case 2	Case 3	Case 4	Case 5	Case 6
P_{ratio}	150	300	450	150	150	850
M_{jet}	1	1	1	2	3	1
$\dot{m}_{jet}$	14.04	28.08	42.12	28.08	42.12	79.56
C_T	2.323	4.653	6.983	6.401	13.196	13.196

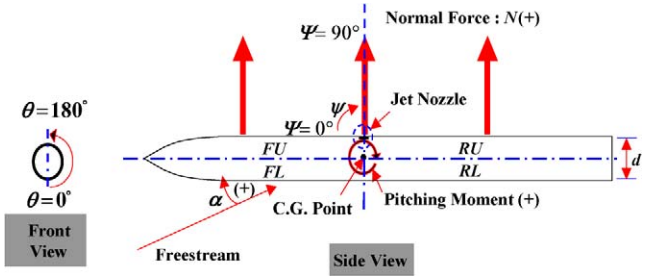

Fig. 11. Nomenclature definition.

Cases 1, 2 and 3 are selected to compare the jet pressure effect while holding the jet Mach number constant. Cases 1, 4 and 5 are compared to determine the jet Mach number effect while holding the jet pressure ratio constant. Cases 2 and 4 have the same mass flow rate increment from Case 1. Cases 3 and 5 also have the same mass flow rate increment from Case 1. Cases 5 and 6 have the same jet thrust. So, the difference between jet Mach number effect and pressure ratio effect with same jet thrust can be observed. For all cases (Cases 1–6), the angle of attack is set to zero.

Furthermore, analyses have been performed for five different circumferential jet locations ($\theta = 0°$, 45°, 90°, 135°, 180°) to determine the effect of the circumferential jet position on the normal force and the pitching moment characteristics of the missile. The freestream and jet flow conditions of these cases are the same as grid system selection case with the angle of attack set to 10°.

3.3. Jet pressure variation: Cases 1, 2 and 3

The pressure contours are shown in Figs. 12 and 13. The calculated results for Cases 1, 2 and 3 are summarized in Table 2. As the pressure ratio increases, the inclination of the barrel shock varies little, but the size of the barrel shock becomes larger. The separation shock and bow shock in front of the nozzle are also moved further forward. Extended high and low pressure regions are shown in Fig. 13, which shows the pressure contour on the surface. This results in increased moment. The pressure distribution plot at the nozzle centerline as shown in Fig. 14 confirms this.

The normal force and the pitching moment are shown almost proportional to the pressure ratio in Table 2. The normal force is always less than the jet thrust due to the low-pressure region behind the nozzle and high-pressure region (at $\theta = 0°$). This high pressure region is caused by a wraparound effect of separation shock. By comparing the normal force and moment at each part of the missile (FU, FL, RU, RL) in Table 2, the high-pressure region in front of the nozzle and the low-pressure

Table 2
The results of calculations (jet pressure variation effect)

	P_{ratio}	C_T	C_N	$C_{N_{FL}}$	$C_{N_{FL}}$	$C_{N_{RU}}$	$C_{N_{RL}}$	C_M	$C_{M_{FU}}$	$C_{M_{FL}}$	$C_{M_{RU}}$	$C_{M_{RL}}$
Case 1	150	2.323	**−2.067**	−0.236	0.099	**0.426**	−0.034	**−0.302**	−0.162	0.053	**−0.701**	0.508
Case 2	300	4.653	**−4.254**	−0.376	0.144	**0.689**	−0.058	**−0.825**	−0.224	0.084	**−1.511**	0.827
Case 3	450	6.983	**−6.440**	−0.470	0.205	**0.903**	−0.095	**−1.660**	−0.330	0.156	**−2.533**	1.046

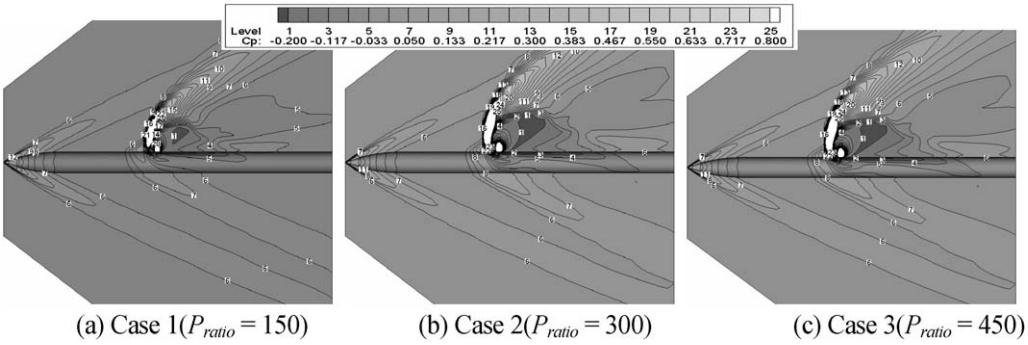

Fig. 12. C_P contour.

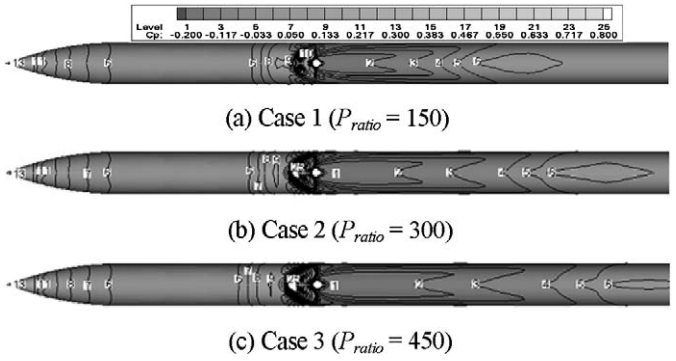

Fig. 13. C_P contour on the surface.

region behind the nozzle produce most of the pitching moment. The low-pressure region behind the nozzle is the primary contributor to the moment generation.

3.4. Jet Mach number variation: Cases 1, 4 and 5

The Mach contour at the symmetry plane and pressure contour on the surface are shown in Figs. 15 and 16, respectively. The calculated results of Cases 1, 4 and 5 are shown in Table 3. The inclination and the size of the barrel shock shape increase with increasing jet Mach number. However, the diameter of the barrel shock near the surface decreases (Fig. 15) due to the jet momentum being proportional to the square of the jet Mach number.

Therefore, the shock standoff distance of bow shock becomes shorter and the high-pressure region in front of the jet nozzle decreases slightly as the jet Mach number increases (Fig. 16). This effect is consistent with the observation by Roger and Chan [9]. Moreover, the low-pressure region immediately behind the nozzle decreases as the jet Mach number increases. The heightened inclination of the barrel shock causes a reduction in the suction effect of the jet and the vortices effect on the surface (Fig. 17). This reduction in vortices effect is due to the separation of the propagated vortices from the surface.

The proportionality of the jet thrust to the normal force and the pitching moment is shown in Table 3. However, less pitch down moment, but higher jet thrust is generated in Case 5 than Case 3 (Table 2) with the same mass flow rate due to the reduced suction effect and effect of vortices.

The relationship of the normal force and the moment coefficients according to the thrust ratio is shown in Fig. 18. The normal force is almost proportional to the jet thrust, but not the moment. It is shown in the case study that the moment is not only a function of the jet thrust, but also jet pressure and Mach number. Since the suction effect and the effect of vortices on the surface are reduced by increasing jet Mach number, the corresponding increased jet thrust produces less pitch down moment than the same thrust produced by increased jet pressure.

3.5. Circumferential jet location effect

Analyses have been performed for several circumferential jet position ($\theta = 0°$, 45°, 90°, 135°, 180°) with angle of attack of 10° to determine the effect of the jet position on the aerodynamic characteristics of the missile with angle of attack. The corresponding pressure contours on the surface are shown in Fig. 19.

A summary of the calculated results and the coefficients of the normal force and the pitching moment for each jet position are shown in Table 4. For each jet position, force and moment are denoted in Fig. 11, i.e. the positive normal force is directed from center of gravity to the jet nozzle direction. Greater normal force loss and pitching down moment are generated when jet nozzle is located at $\theta = 0°$ than $\theta = 180°$ as shown in Fig. 20. However, maximum normal force and minimum pitching down moment are generated when jet nozzle is located at $\theta = 90°$. This is caused by the largest high pressure region on the rear body upper surface behind the nozzle in case of $\theta = 90°$. This

Table 3
The results of calculations (jet Mach number variation effect)

	M_{jet}	C_T	C_N	$C_{N_{FU}}$	$C_{N_{FL}}$	$C_{N_{RU}}$	$C_{N_{RL}}$	C_M	$C_{M_{FU}}$	$C_{M_{FL}}$	$C_{M_{RU}}$	$C_{M_{RL}}$
Case 1	1	2.323	**−2.067**	−0.236	0.099	**0.426**	−0.034	**−0.302**	−0.162	0.053	**−0.701**	0.508
Case 4	2	6.401	**−6.028**	−0.373	0.118	**0.661**	−0.032	**−0.981**	−0.187	0.059	**−1.686**	0.833
Case 5	3	13.196	**−12.837**	−0.436	0.122	**0.641**	0.032	**−1.613**	−0.197	0.059	**−2.077**	0.602

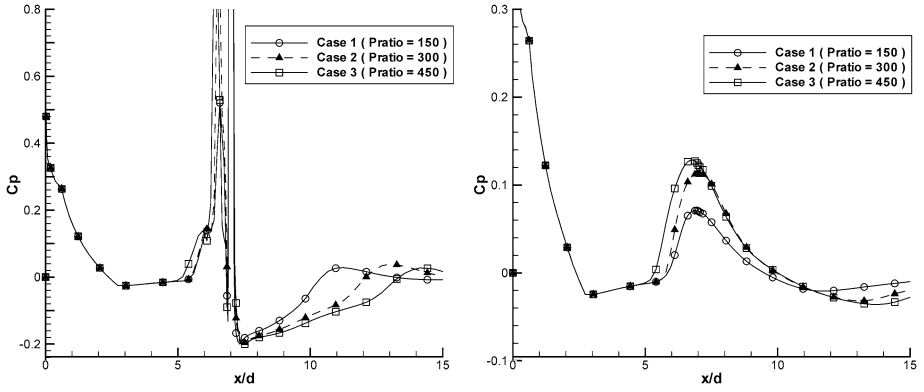

(a) θ=180° (b) θ= 0°

Fig. 14. C_P plots at $\theta = 0°, 180°$.

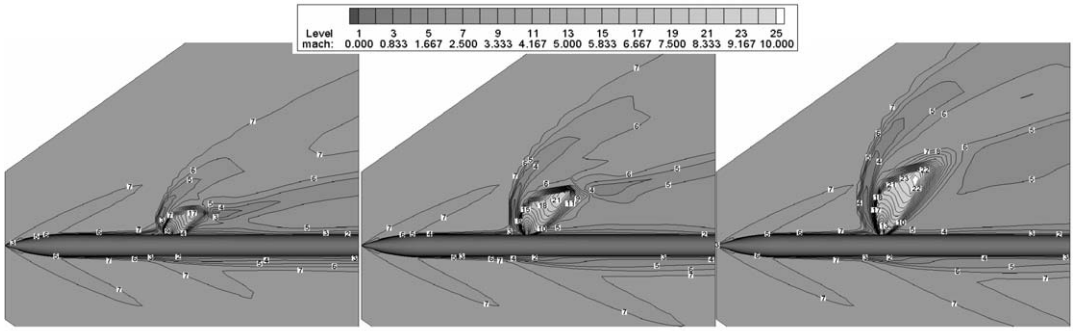

Fig. 15. Mach number contour.

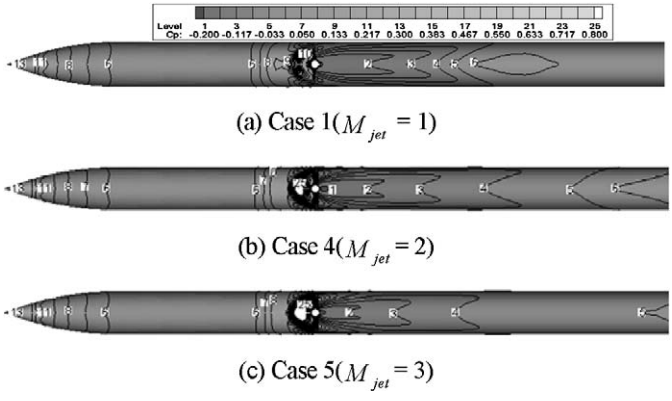

Fig. 16. C_P contour on the surface.

region of high pressure contributes to the increase of the normal force, while simultaneously decreasing the pitching down moment. This high pressure region on the rear body upper surface is created by a strong bow shock caused by the freestream as shown in Fig. 19. The same freestream causes a bend in the jet, which leads to a low pressure region being generated at the opposite end of the nozzle. Hence, the lateral jet should be operated by considering these varying aerodynamic characteristics.

4. Conclusions

A computational study of supersonic flow around a lateral jet controlled missile has been performed. Three-dimensional Navier–Stokes computer code has been developed and validated by comparing the analytical result with the experimental data. Several cases with different jet pressure, jet Mach number, jet mass flow rate, and circumferential jet position were selected to investigate the detailed flowfield, the shock formation, and the surface pressure distribution of the lateral jet controlled missile. Aerodynamic analyses were performed to gage the effect of these factors on the normal force and pitching moment coefficients.

Table 4
The comparison of calculated results for jet location effect (jet effect only = total value − α effect)

θ	C_N	$C_{N_{FU}}$	$C_{N_{FL}}$	$C_{N_{RU}}$	$C_{N_{RL}}$	C_M	$C_{M_{FU}}$	$C_{M_{FL}}$	$C_{M_{RU}}$	$C_{M_{RL}}$
0°	**−1.763**	−0.23	0.027	**0.465**	−0.008	**−1.231**	−0.063	0.010	**−1.162**	−0.015
45°	**−1.767**	−0.202	0.022	**0.364**	0.036	**−0.8**	−0.058	0.005	**−0.763**	0.017
90°	**−1.956**	−0.169	0.036	**0.193**	0.0	**0.178**	−0.08	0.017	**−0.281**	**0.522**
135°	**−1.950**	−0.177	0.03	**0.174**	0.039	**−0.473**	−0.143	0.015	**−0.503**	0.158
180°	**−1.824**	−0.168	0.036	**0.263**	0.062	**−0.662**	−0.129	0.014	**−0.609**	0.063

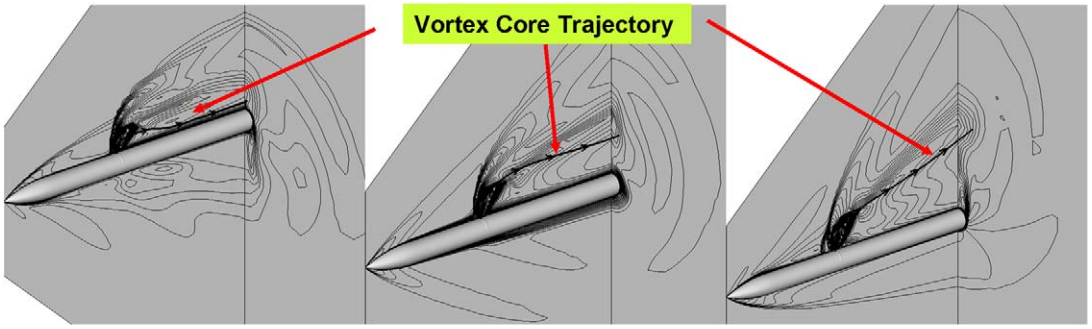

Fig. 17. Mach number contour and vortices.

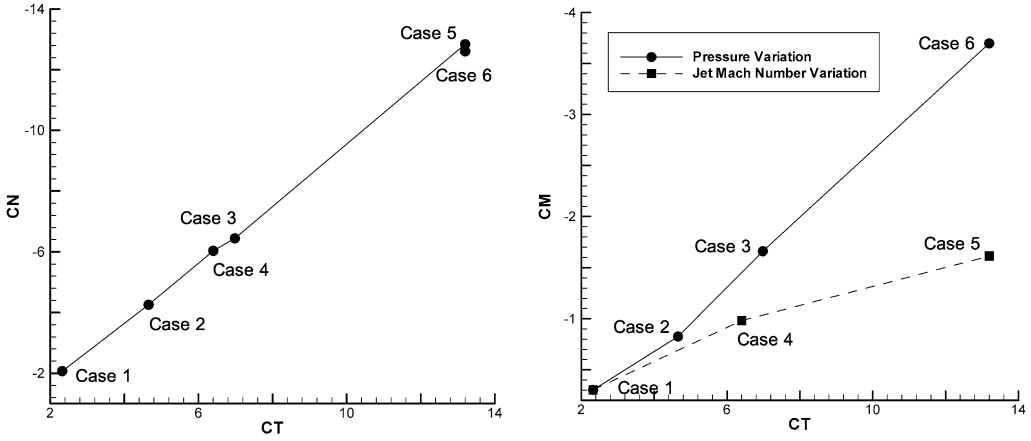

(a) C_N *vs.* C_T (b) C_M *vs.* C_T

Fig. 18. C_N, C_M vs. C_T plots.

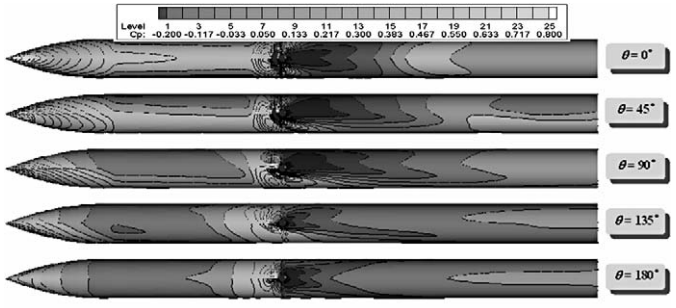

Fig. 19. C_P contour on the surface.

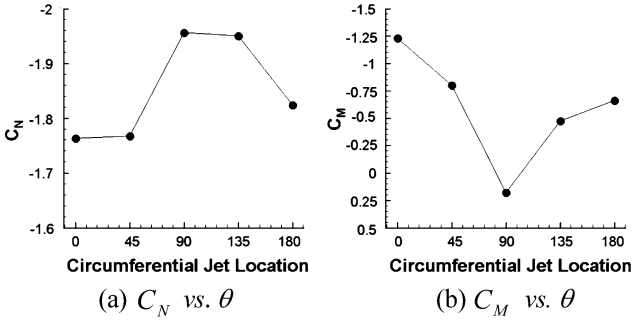

(a) C_N *vs.* θ (b) C_M *vs.* θ

Fig. 20. C_N, C_M vs. circumferential jet location plots.

The normal force was almost proportional to the jet thrust but shock interactions induced thrust loss. However, the pitching moment deviates from such a pattern for varying jet pressure and jet Mach number values. When increasing the jet pressure only, the pitching down moment increases proportionally. When increasing jet Mach number only, the inclination of the

barrel shock increases. This causes reduction in the pitch down moment increment. Thus, increasing jet Mach number is preferred in obtaining higher jet thrust, rather than increasing jet pressure ratio.

The aerodynamic force and moment acting on the missile are varied according to the jet location. It is observed that in the case with $\alpha = 10^\circ$, minimum normal force loss and pitching moment are generated when the jet is ejected at $\theta = 90^\circ$. Thus, an angle of yaw is more effective for missile control by side jet than an angle of attack.

The low-pressure region behind the jet nozzle is a primary contributor to pitch down moment generation and normal force loss. Thus, it is evident that for efficient lateral jet attitude control system design further study on reducing the low-pressure region is necessary.

Acknowledgement

This work was supported by grant number ADD-03-01-01 from the Basic Research Program of the Agency for Defense Development.

References

[1] F.S. Billig, R.C. Orth, M. Lasky, A unified analysis of gaseous jet penetration, AIAA J. 9 (6) (1971) 1048–1058.

[2] J. Brandeis, J. Gill, Experimental investigation of side-jet steering for supersonic and hypersonic missiles, J. Spacecraft and Rockets 33 (3) (1996) 346–352.

[3] R. Chamberlain, Calculation of three-dimensional jet-interaction flowfields, AIAA Paper 90-2099, 1990.

[4] E.L. Fleeman, Propulsion considerations in tactical missile design, in: J.S. Przemieniecki (Ed.), Tactical Missile Design, in: Education Series, AIAA, Reston, 2001, pp. 59–88.

[5] C. Hirsch, Second-order upwind and high-resolution schemes, in: Numerical Computation of Internal and External, vol. 2: Computational Method for Inviscid and Viscous Flow, John Wiley & Sons, 1988, pp. 493–594, Chapter 21.

[6] K.A. Hoffmann, S.T. Chiang, Turbulent flow and turbulence models, in: Computational Fluid Dynamics, vol. III, fourth ed., Engineering Education System, Wichita, 2000, pp. 20–115.

[7] R.G. Lacau, M. Robert, The use of lateral jet control at aerospatiale, in: Proceedings of the Missile Aerodynamics Near Conference on Missile Aerodynamics, Nielsen Engineering & Research, Monterey, CA, October–November, 1988, pp. 11.1–11.15.

[8] E.W. Perkins, L.H. Jorgensen, Comparison of experimental and theoretical normal-force distributions (including Reynolds number effects) on an ogive-cylinder body at Mach number 1.98, NASA-TN-3716, May 1956.

[9] R.P. Roger, S.C. Chan, Parameters affecting penetration of a single jet into a supersonic crossflow: A CFD study – II, AIAA-1998-425, January 1998.

[10] R.P. Roger, S.C. Chan, S.C. Praharaj, Parameters affecting penetration of a single jet into a supersonic crossflow: A CFD study – I, AIAA-1997-2225, June 1997.

[11] B. Srivastava, Computational analysis and validation for lateral jet controlled missiles, J. Spacecraft and Rockets 34 (5) (1997) 584–592.

[12] S. Yoon, D. Kwak, Three-dimensional incompressible Navier–Stokes solver using lower-upper symmetric-Gauss–Seidel algorithm, AIAA J. 29 (1991) 874–875.